Journal of Materials Chemistry C

Accepted Manuscript

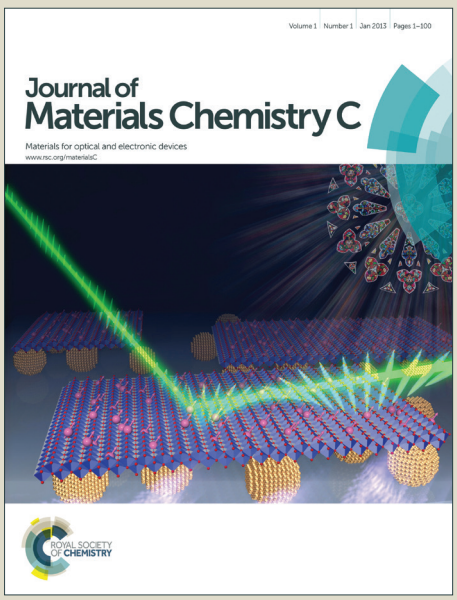

ROYAL SOCIETY OF CHEMISTRY

www.rsc.org/materialsC

Journal of Materials Chemistry C

Dynamic Article Links ►

Cite this: DOI: 10.1039/c0xx00000x

www.rsc.org/xxxxxx

Paper

The coupled effect of oxygen vacancy and Pt on the photoelectric response of tungsten trioxide films

Chaoqun Yang, Qiang Zhu, Tao Lei, Huayao Li, Changsheng Xie, *

Received (in XXX, XXX) Xth XXXXXXXXX 20XX, Accepted Xth XXXXXXXXX 20XX

DOI: 10.1039/b000000x

In this paper, four kinds of WO_3 films, namely, Pt-loaded hydrogenation WO_3, Pt-loaded WO_3, hydrogen-treated and untreated WO_3 films were synthesized and their photoelectric properties were investigated at room temperature. The quantitative results showed that the gas-sensitized WO_3 film in formaldehyde exhibited much higher photocurrent than that in air. In addition, the sensitivity of Pt-loaded hydrogenation WO_3 to formaldehyde reached to 15.8 which was nearly 15 times higher than that of the others. Moreover, the Pt-loaded hydrogenation WO_3 shows excellent electrical response towards the formaldehyde in the darkness. The intriguing performance of the Pt-loaded hydrogenation WO_3 film indicates an efficient coupled effect of the oxygen vacancies and Pt. The results provide the potential for improving efficiency of photoelectric sensitive devices by coupling two modification mechanisms. To explain the response characteristics of the four kinds of WO_3 films, a schematic diagram of the band bending and spill over model are proposed.

1 Introduction

Photocurrent measurement is now considered to be the most valuable characterization method in characterizing the charge transfer and separation since the photocurrent can be a probe for straightforward interpretation of the competition between photogeneration, recombination, and trapping [1-3]. Nowadays, testing the photocurrent to figure out the carrier transport mechanism in the photoresponse process has attracted extensive attention [4-7]. The overall photoresponse process in a semiconductor can be summarized as the successive procedure of the solar absorption, charge-carriers separation, and charge-carriers transport. Generally speaking, one kind of material with wide absorption wavelength range, effective charge-separation and high mobility will exhibit excellent photoelectric response performance. Therefore, the photoresponse characteristics of semiconductors can be modulated by adjusting the above three processes. Recently, much effort has been done to modulate the photoresponse characteristics of metal oxide semiconductor (MOS). For example, to increase the absorption wavelength range, the semiconductor materials annealed in hydrogen to introduce oxygen vacancy have attracted much attention. Chen et al. reported that TiO_2 could absorb NIR and visible light after introducing oxygen vacancy by hydrogenation [8]. Li et al. reported a full-spectrum absorption effect of hydrogen treated WO_3 due to the introduction of oxygen vacancy [9]. Zhu et al. reported that via annealing in a hydrogen atmosphere, the ZnO exhibited an obvious optical absorption in the visible region [10].

To enhance the separation efficiency of photoexcited electron-hole pairs, surface decorations have been used extensively. For example, Solarska et al. proved that the silver nanoparticle could induce photocurrent enhancement at WO_3 photoanodes [11]. Lee et al. reported Ag grid induced photocurrent enhancement in WO_3 [12]. Furthermore, it is well known that the photocurrent is a long-term process which is limited by the carrier mobility [10,13]. Due to the mobility has the following expression: $\mu^* = \mu_0 \exp(-\phi_B / k_B T)$ [13], where the μ^* and μ_0 are the effective mobility over the sample and the intrinsic mobility inside the grain and is the barrier height at the Grain boundary (GB). This equation means that, as ϕ_B increases, the μ^* decreases. Therefore, when the temperature is constant, adjusting the barrier height at the GB resulting from band bending is a good method to modulate the carrier mobility. Recently, many researchers have also done a lot of work in this field [14-16]. Zou et al. reported that the ZnO modified with CdS showed an enhancement of photocurrent resulting from the decrease of grain boundary barrier height [15]. Zangwill and his coworkers reported that when the metal and semiconductor were in contact, the band bending would be formed near the semiconductor due to the difference of work function of metal and semiconductor [17]. It is the above three processes that the photocurrent is influenced, therefore we can study the photocurrent to investigate the charge-transport process in the semiconductor.

WO_3 is of great interest for various technological applications from electrochromic devices to gas sensors [18-20] because of its distinctive optical, electrical, structural, and defect properties. As

an important n-type semiconductor with a relatively narrow gap (2.4 -2.8eV), WO_3 can theoretically utilize visible-light [21]. However, its high recombination rate of e^- - h^+ pairs and relatively low reduction potential limit its application [22-23]. Therefore, overcoming the shortcomings in WO_3 during the photoresponse process remains an important subject for developing the WO_3 photoelectric devices.

Recently, many efforts have been devoted to developing new strategies for further improving the photoelectric property of WO_3 via the introduction of oxygen vacancy and surface modification [11, 24-25]. Through the introduction of oxygen vacancy, the solar absorption characteristics of WO_3 have been improved. Our previous work has found that the WO_3 with more oxygen vacancies shows high photosensitivity to infrared light resulting from the formation of the defect band in the band gap which makes the activation energy of electrons hopping from the defect level to the conduction band decrease [5]. Through surface modification, the charge- separation and charge carrier mobility have been adjusted. Pt loading on the WO_3/p-Si can induce photocurrent enhancement reported by Yoon and his coworkers [26]. Although much work has been done to investigate the influence of surface decoration and oxygen vacancy introduction on the photoelectricity response of WO_3 from the processes of carrier generation and recombination, respectively, there are only few reports concerning the combination of the both methods. So what the properties of WO_3 would happen if we combine surface decoration and oxygen vacancy adjustment? What is the mechanism of charge-transport in the WO_3? Can we achieve the synergistic effect of the both?

In order to make a study on these questions, we developed a Pt-loaded hydrogenation WO_3 film and focused on the comparative study of different treated WO_3 films on their photoelectric responses at room temperature under light illumination and dark state. The photogenerated carrier transport mechanism in different WO_3 films and the roles of oxygen vacancies and Pt on the carrier generation and recombination process were emphatically discussed.

2 Experimental details

The analytical grade precursor chemicals used were sodium tungstate dihydrate ($Na_2WO_4{\cdot}2H_2O$, 99% Aldrich), Ammonium oxalate ($(NH4)_2C_2O_4$, 99.5% Sinopharm), 3M hydrochloric acid (HCl, Sinopharm), absolute ethanol (C_2H_5OH, Sinopharm), and deionized (DI) water. All chemicals were used without further purification.

2.1 Material preparing

In the preparation of the material, a three-step synthesis process was involved. Firstly, we prepared the as-grown WO_3 nanoplate array on the Fluorine doped Tin oxide glass (FTO) by hydrothermal method. In order to investigate the photoelectric properties of WO_3 films, the ablated Fluorine doped Tin oxide (FTO) glass was used as the electrode in this study and the ablated FTO electrode was referred to Zhu and his coworkers [27]. Before growing the WO_3 nanoplates, the FTO must be conducted a precleaned by ultrasonic treatment in detergent, de-ionized water, acetone and methanol. The WO_3 films were coated onto FTO glass without a seed layer according to the method proposed by Yang and his coworkers [28]. Then the FTO glasses were immersed into the growth-promoting media and guaranteed to be vertical to the wall of the Teflon-vessel. After the autoclave was sealed, the hydrothermal synthesis was carried out at 160 °C for 2 h. After that, the autoclave was allowed to cool down to room temperature in the oven, then the FTO glasses were taken out and washed with deionized water and methyl alcohol in sequence and finally dried at 80 °C in air for 12 hours.

Secondly, we prepared the hydrogen-treated samples and air-treated samples through annealing the samples synthesized in the first step in hydrogen (1 bar, 5% H_2, 95% Ar, 135 mL/min flow) and in air at 450 °C for 2 h, respectively.

Thirdly, the hydrogen treated samples were loaded with Pt by an impregnation method in which the hydrogen-treated WO_3 film was immersed into the chloroplatinic acid (0.000429 g/mL) for 10 min. Then, the film was calcined in air at 350 °C for 2 h. For the convenience of discussion, the material is denoted as Pt-H-WO_3. The air -treated samples were loaded with Pt using the same method which is denoted as Pt-WO_3. In this paper, the air-treated WO_3 and hydrogen-treated WO_3 are denoted as U-WO_3 and the H-WO_3, respectively. The preparation procedure of the four kinds of WO_3 is illustrated in Fig. 1.

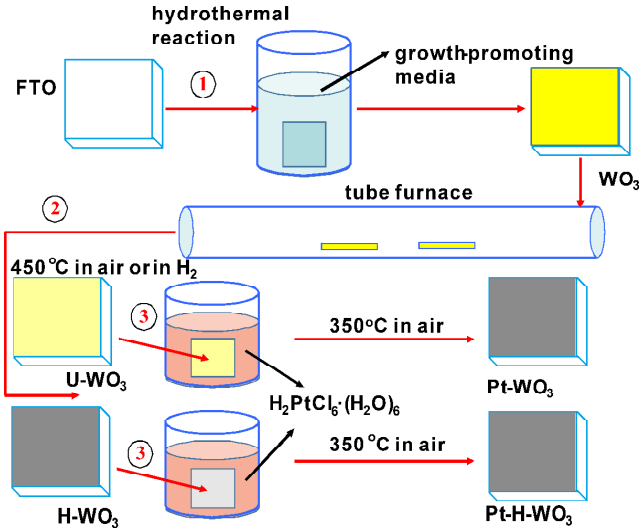

Fig. 1. Schematic illustration for the fabrication of the four kinds of WO_3 films: U-WO_3 (untreated WO_3) films, H-WO_3 (hydrogen-treated WO_3) film, Pt-WO_3 (Pt-loaded WO_3) film and Pt-H-WO_3 (Pt-loaded hydrogenation WO_3 film).

2.2. Structural characterization

XRD analysis was carried out on an X-ray diffractometer (X'Pert PRO, PANalytical B.V.) using Cu Kα radiation in the 2θ ranges from 20 to 80°. The absorbance of the films was measured with a UV/visible spectrophotometer (Lambda35 PerkinElmer) at room temperature within the wavelength range of 200 ~ 1100 nm. The surface morphologies were studied using FESEM (Hitachi S-4800 FE-SEM). X-ray photoelectron spectroscopy analyses were performed in a VG ESCA III spectrometer using the Al Kα radiation. The binding energy reference was the C 1s peak at 285.0 eV. The Photoluminescence (PL) spectra were taken in the wavelength range 200 ~ 1000 nm by using a Xe lamp as the excitation light source (excitation at 325 nm) at room

temperature. The Raman spectra were measured from 50 to 1000 cm-1 using a 50 mW and 532 nm wavelength Ar green laser.

2.3. Photoelectric response measurement

The photoelectric properties of WO_3 films were measured by a test platform developed by our laboratory [29]. The test platform is mainly composed of, test chamber, light source and signal processing system. This platform could evaluate 4 samples every time. In this study, a total test process lasted for 3000 s containing 5 cycles. The details of the test process in air were as follows. First, let the dry air continuously flow into the test chamber to keep the relative humidity constant (< 20%) and then the test gas (dry air or 100 ppm formaldehyde) was introduced into the test chamber. The bias of 1 v used to separate electron-hole pairs was loaded at 15 s and unloaded at 3000 s. In the testing process, we turn the light on at 30 s for the first time and turn the light off at 300 s, then 600 s on, 900 s off, by analogy, until the end of the fifth cycle. The flow of air stream was controlled as 200 mL/min by a mass flow controller. The blue (465 nm) LED array lights (Light Emitting Diode, Shenzhen Ti-Times Co.) was used for illuminating the samples as light sources at 30 s. The response of WO_3 toward formaldehyde under dark state was tested. The testing process was set to a mode that formaldehyde was in at 15 s and out at 600 s, then 1200 s in, 1800 s out, by analogy, until the end of the fourth cycle.

3. Results and discussion

3.1. Characterization of the WO_3 films

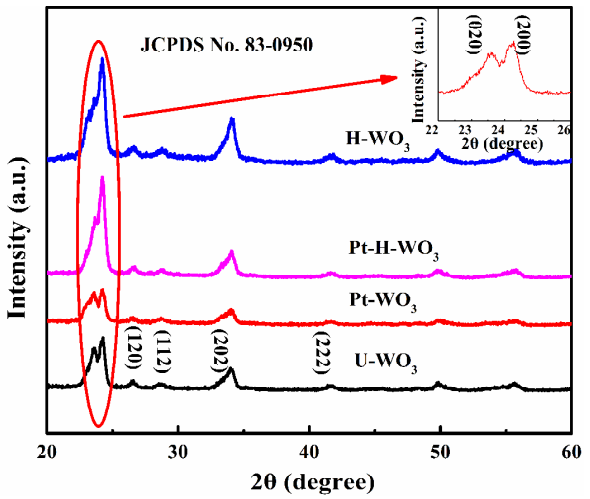

Fig. 2. XRD spectra of the four kinds of WO_3 films: U-WO_3 (untreated WO_3) films, H-WO_3 (hydrogen-treated WO_3) film, Pt-WO_3 (Pt-loaded WO_3) film and Pt-H-WO_3 (Pt-loaded hydrogenation WO_3 film).The inset shows the magnified spectra of the red rectangle.

Fig. 2 shows the XRD spectra of the four WO_3 films, namely, U-WO_3, Pt-WO_3, H-WO_3 and Pt-H-WO_3. All the diffraction peaks in the XRD pattern can be indexed to a monoclinic WO_3 phase (JCPDS No. 83-0950). The surface morphology of the as-prepared WO_3 samples were investigated by SEM. As shown in Fig. 3, four WO_3 films are all composed of WO_3 nanoplates. Fig. 3(a), 3(b), 3(c) and 3(d) are top-view images of the four WO_3 films. The average length and thickness of the platelets determined from the SEM images are ~ 500nm and ~100nm, respectively. Fig. 3(e) shows the cross-sectional image of WO_3. From Fig. 3(e), we can see that the thickness of the film is about 800 nm. Both of the XRD and SEM results prove that the four kinds of WO_3 films exist the similar phase structures and morphologies.

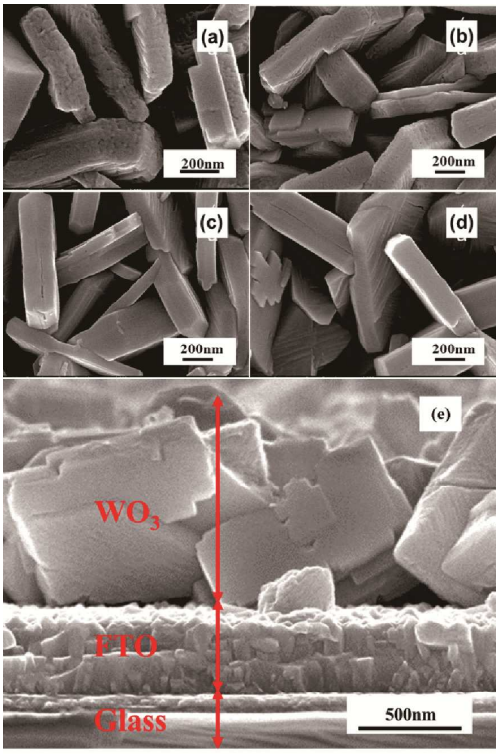

Fig. 3. SEM images of the four kinds of WO_3 films: U-WO_3 (untreated WO_3) films (a); H-WO_3 (hydrogen-treated WO_3) film (b); Pt-WO_3 (Pt-loaded WO_3) film (c); Pt-H-WO_3 (Pt-loaded hydrogenation WO_3) film (d); the cross-sectional image of U-WO_3 (untreated WO_3) thin film (e).

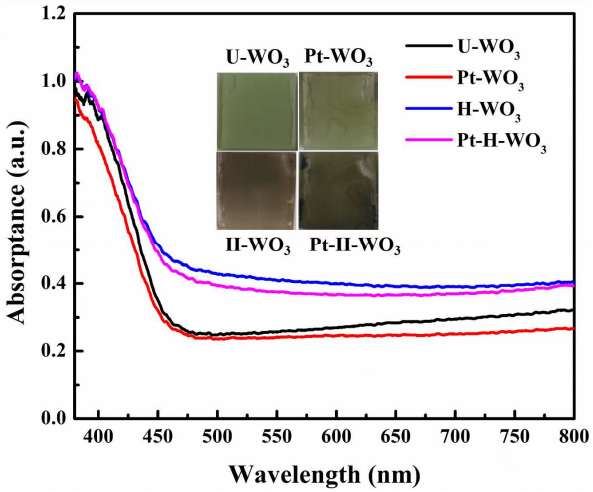

Fig. 4. UV -Vis absorption spectra of four kinds of WO_3 films: U-WO_3 (untreated WO_3) film; H-WO_3 (hydrogen-treated WO_3) film; Pt-WO_3 (Pt-loaded WO_3) film and Pt-H-WO_3 (Pt-loaded hydrogenation WO_3) film. The inset shows the color changes of the four kinds of WO_3 films.

Fig. 4 shows the UV-vis absorption spectra of the U-WO_3, Pt-WO_3, H-WO_3 and Pt-H-WO_3 films. From the UV–vis spectra, it can be seen that the four WO_3 films show a fairly identical

absorbance in the UV region (< 400 nm) and a high optical absorbance in the region of 400 - 800 nm. That is to say, in the whole spectral range, all WO_3 films prepared by us exhibit an absorbance to some degree. However, the H-WO_3 and Pt-H-WO_3 show higher optical absorbance than that of U-WO_3 and Pt-WO_3 films in the visible light region. Commonly, the optical absorption of nanocrystals is assigned to the electronic transitions involving the conduction band, the valence band, and the various intrinsic defect levels [27]. The defect energy levels lying within the band gap will make the low energy light absorbed by WO_3. For the four kinds of WO_3 films, oxygen vacancies are much more than other defects. There have been reports that hydrogen treatment can effectively extend the visible light absorption of MOS, such as ZnO [27], TiO_2 [8], WO_3 [24] due to the introduction of oxygen vacancies. These oxygen vacancies can form defect levels lying within the band gap [27].This is maybe attributed to the higher absorbance of H-WO_3 and Pt-H-WO_3 in the visible light range. As shown in the inset of Fig. 4, the colors of H-WO_3 and Pt-H-WO_3 turn into dark blue from whity-yellow U-WO_3 and Pt-WO_3 films. The same phenomenon of color change of WO_3 has been reported by others [20, 30]. The values of the band gaps for U-WO_3, Pt-WO_3, H-WO_3 and Pt-H-WO_3 are 2.57 eV, 2.58 eV, 2.47 eV and 2.47 eV, respectively. The band gap energies of the three samples are calculated according to the equation $\alpha hv = A(hv - Eg)^n$ [31]. Where A is a constant, hv is the incident photon energy, E_g is the band gap energy, and n is equal to 2 for WO_3. It is reported that the increasing of oxygen vacancies results in a narrowing band gap [32]. Therefore, the lower band gaps of H-WO_3 and Pt-H-WO_3 than that of U-WO_3 and Pt-WO_3 films may be assigned to the larger numbers of oxygen vacancies in the H-WO_3 and Pt-H-WO_3 films.

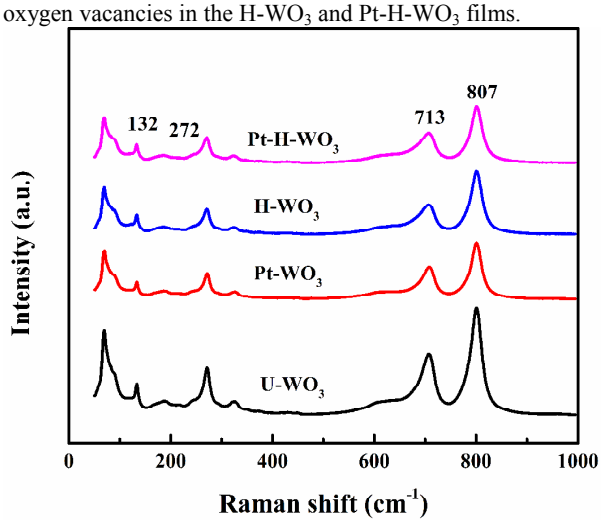

Fig. 5. Raman spectra of four WO_3 films: U-WO_3 (untreated WO_3) films; H-WO_3 (hydrogen-treated WO_3) film; Pt-WO_3 (Pt-loaded WO_3) film and Pt-H-WO_3 (Pt-loaded hydrogenation WO_3 film).

The vibration modes of the WO_3 samples are investigated by Raman spectra, which are shown in Fig. 5. The Raman spectra are similar to each other from Fig. 5. Two bands at 713 cm^{-1} and 808 cm^{-1} both result from O-W^{6+}-O stretching modes [33-34]. The band at 272 cm^{-1} is assigned to the bending vibrations of W-O-W [35]. As supported by available literature [33,36], these bands are characteristic of monoclinic WO_3, confirming the results obtained by XRD that the four WO_3 films belong to monoclinic phases.

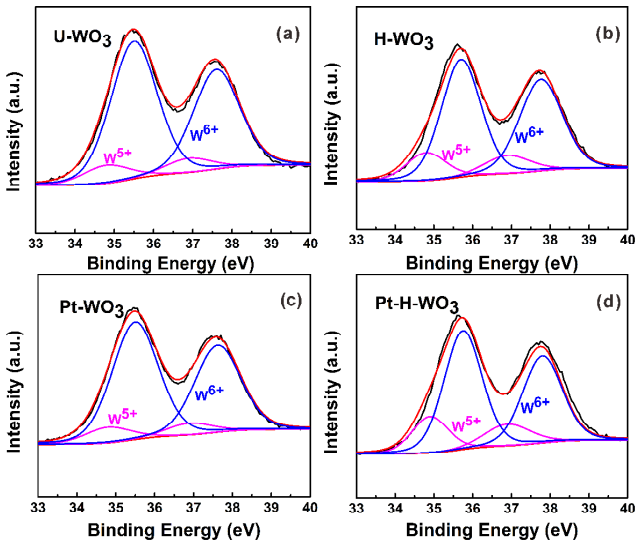

Fig. 6. X-ray photoelectron spectroscopy spectra of the W 4f for the four kinds of WO_3 films: U-WO_3 (untreated WO_3) films (a); H-WO_3 (hydrogen-treated WO_3) film (b); Pt-WO_3 (Pt-loaded WO_3) film (c); Pt-H-WO_3 (Pt-loaded hydrogenation WO_3) film (d).

In order to understand the chemical compositions and the defect states of the WO_3, XPS analysis was performed on the different WO_3 samples. Fig. 6 shows the spectra of W 4f and the results of their decomposition into peaks of the samples. According to the reported procedure for fitting the spin orbit doublet of W 4f [37-38], 2 doublets were used to fit the W 4f core level. For W^{5+}-states of oxide, the main doublet (W $4f_{7/2}$) is centered at 34.8 eV and for W^{6+}-states of oxide, the maxima of peak couples correspond to W $4f_{7/2}$ is centered at 35.7 eV. The parameters of spin–orbit separation is E_p ($4f_{5/2}$–$4f_{7/2}$) = 2.1 eV and the intensity ratio is $I_{4f5/2}/I_{4f7/2}$= 0.75. As listed in Table 1, the relative integrated intensity ratios of the W^{5+} and W^{6+} calculated from W 4f fitted peaks for the four films can be obtained. The percentages of W^{5+} are 11.6%, 11.8%, 18.2% and 22.4% for U-WO_3, Pt-WO_3, H-WO_3 and Pt-H-WO_3, respectively. Since the reduction of W^{6+} to W^{5+} relates to the changes of oxygen. Therefore, the concentration of W^{5+} can reveal the content of oxygen vacancies indirectly. We can deduce that the order of the concentrations of oxygen vacancies of the four WO_3 films is: Pt-H-WO_3 > H-WO_3 > Pt-WO_3 > WO_3. From Fig. 6, we can find that there are some slight peak shifts for W^{5+} and W^{6+}, especially W^{5+} peak between H-WO_3 and Pt-H-WO_3. This is attributed to the dual roles of Pt and hydrogenation which make the electron cloud density on the surface of the WO_3 decreased. Therefore the peaks for W^{5+} and W^{6+} shift towards to the high binding energy for Pt-H-WO_3.

To gain more insight into the oxygen vacancies, the O 1s spectra of the four WO_3 films are shown in Fig. 7. The O 1s spectra are carefully deconvoluted into 3 peaks (O_a, O_b, O_c) by using Gaussian fitting. According to the results reported by other researchers [37-39], the O_a peak at 530.2 eV is attributed to the inherent O associated with W. The O_b peak at 531.5 eV is attributed to the O^{2-} ions in the oxygen-deficient regions and the

O_c peak at 532.5 eV due to the contaminated O on the surface of the thin film. The relative integrated intensity percentages of the different oxygen species calculated from O 1s fitting peaks are listed in the Table 2. The change in the intensity of O_b peak is in connection with the variations in the concentration of the oxygen vacancy [40]. According to XPS result, it is evident that all of the WO_3 films contain some V_O defects and absorbed oxygen. And from Table 2, the absorbed oxygen on the surface of WO_3 increases with oxygen vacancy increasing. Many researchers have reported that the presence of oxygen vacancies on the surface results in increasing adsorption of gas molecules [41-42]. Therefore, the H-WO_3 and Pt-H-WO_3 absorb more oxygen on the surface.

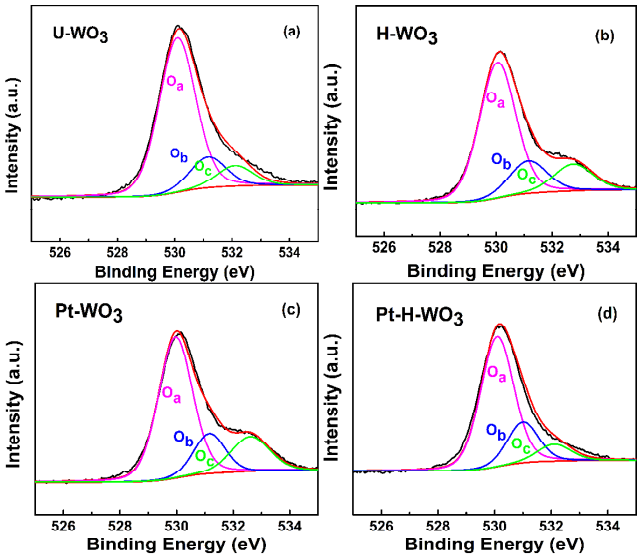

Fig. 7. X-ray photoelectron spectroscopy spectra of the O 1s for the four kinds of WO_3 films: U-WO_3 (untreated WO_3) films (a); H-WO_3 (hydrogen-treated WO_3) film (b); Pt-WO_3 (Pt-loaded WO_3) film (c); Pt-H-WO_3 (Pt-loaded hydrogenation WO_3) film (d).

Table 1 The relative integrated intensity percentages for the W^{5+}, W^{6+} calculated from W 4f fitting peaks of the four kinds of WO_3 films.

Sample	W^{5+}, E_p W $4f_{7/2}$ (%)	W^{6+}, E_p W $4f_{7/2}$ (%)
U-WO_3	11.8	88.2
Pt-WO_3	11.6	88.4
H-WO_3	18.2	81.8
Pt-H-WO_3	22.4	77.6

Table 2 The relative integrated intensity percentages for the different oxygen species calculated from O 1s fitting peaks of the four kinds of WO_3 films.

Sample	O_a (%)	O_b (%)	O_c (%)
U-WO_3	75.14	14.87	9.99
Pt-WO_3	72.96	16.9	12.14
H-WO_3	66.45	19.06	14.49
Pt-H-WO_3	65.23	19.63	15.14

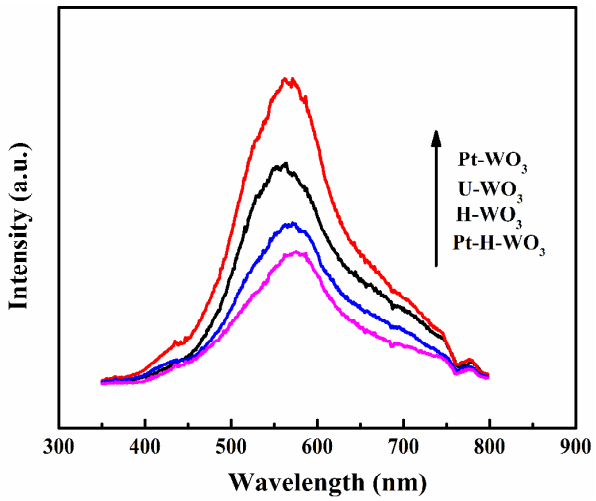

Fig. 8. The PL spectra of the four kinds of WO_3 films under the excitation of UV light at 325 nm. U-WO_3 (untreated WO_3) films; H-WO_3 (hydrogen-treated WO_3) film; Pt-WO_3 (Pt-loaded WO_3) film and Pt-H-WO_3 (Pt-loaded hydrogenation WO_3 film).

For better understanding the presence of defects in the samples, PL spectra of the samples at room temperature were tested, which was shown in Fig. 8. It can be obviously seen that the photoluminescence intensities of the four kinds of WO_3 films are different. The main peaks centered at ~ 550 nm in the PL spectra for all of the samples originate from the localized states and defects in the band gap that is verified by our previous work [5]. In general, the lower PL intensity indicates the lower recombination rate of photogenerated electron-hole pairs [43]. According to the PL spectra, the Pt-WO_3 shows the highest emission intensity, while the Pt-H-WO_3 exhibits the lowest intensity among the four samples indicating a much repressed recombination rate. It is well known that the oxygen vacancies which act as electron traps can prevent photogenerated carriers from rapid recombination. And Pt can not only act as an electron sink to capture electrons suppressing the recombination of electrons and holes, but also can discharge electrons to recombine with holes or react with reactants [44]. For Pt-WO_3, the Pt mainly acts as a recombination center resulting in a high recombination rate. While for Pt-H-WO_3, Pt acts as an electron sink. The different roles of Pt in Pt-WO_3 and Pt-H-WO_3 come from the different band structures of them. This has an important relationship with whether hydrogenation or not. For WO_3, the hydrogen treatment causes the formation of large amounts of oxygen vacancies. That makes more oxygen adsorption on the surface of hydrogen-treated WO_3 than that of untreated WO_3. Those oxygen molecules acting as strong acceptors to capture the free electrons and bend the energy bands upward. The electrons will transfer from the WO_3 to the lowest unoccupied molecular orbital (LUMO) of the molecule until E_F decreases to the same energy as that of the LUMO level [47]. In this process, the E_F of WO_3 decreases. The E_F of hydrogen-treated WO_3 is lower than that of untreated WO_3 duo to the larger oxygen vacancies in the hydrogen-treated WO_3. When Pt loaded, the electrons will

transfer from WO_3 to the Pt until the Fermi levels of Pt ($E_{F,Pt}$) and WO_3 ($E_{F,s}$) are aligned. The lager ΔE_F ($E_{F,s}$-$E_{F,Pt}$), the more electrons transferring to Pt. From this we can infer that there are more electrons transferring to Pt for Pt-WO_3 than that of Pt-H-WO_3. Thus for Pt-WO_3, a large number of electronic gather on the Pt and quickly recombine with holes. While for Pt-H-WO_3, a small amount of electrons transfer to the Pt. These electrons are captured in the Pt and can't quickly recombine with holes. This moment, the role of Pt is electron sink. Meanwhile, oxygen vacancies acting as electron traps can prevent photogenerated carriers from rapid recombination. It is the synergistic effect of oxygen vacancy and Pt that makes the Pt-H-WO_3 show a very low recombination rate.

3.4. Photoelectric response

Fig. 9 shows the five consecutive cycles of photocurrent-time curves of the four kinds of WO_3 films in air. Take a first look at the responses of the four WO_3 films, the photocurrents of the four WO_3 films increase rapidly upon blue light illumination. When the light is off, the photocurrents reduce slowly and can't return to its original value. The phenomenon which the photocurrents reduce slowly suggests that carrier traps exist within the band gap [45]. Both the PL and the XPS results demonstrate that there is a certain amount of oxygen vacancies which usually act as electron traps in the four samples. These electron traps make some electrons captured, resulting in an enhancement of the carrier lifetime [30,45], which make the photocurrents reduce slowly. Here, the maximum photocurrent values at each cycle in air are extracted and the photo-generated current defined by $I= I_{off}-I_{on}$ are calculated, which are depicted in Fig. 10. As shown in Fig. 9 and Fig. 10, three main results can be obtained.

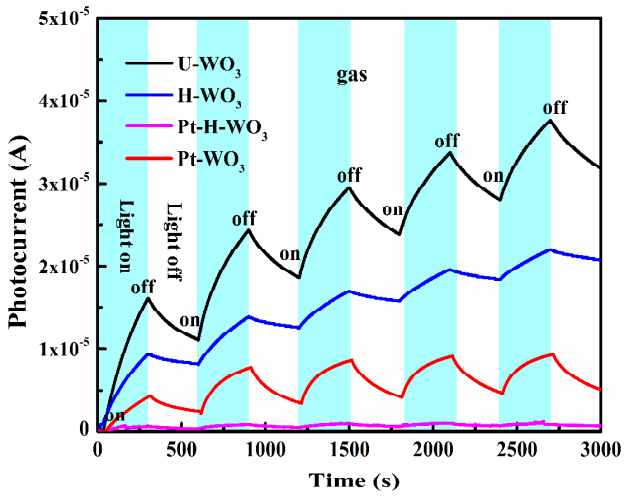

Fig. 9. The photoelectric response curves of the four kinds of WO_3 films in the air under the blue light illumination. U-WO_3 (untreated WO_3) films; H-WO_3 (hydrogen-treated WO_3) film; Pt-WO_3 (Pt-loaded WO_3) film and Pt-H-WO_3 (Pt-loaded hydrogenation WO_3 film).

Firstly, after scores of cycles, the photocurrent amplitudes gradually increase, result in the ladder-like photocurrent-time curves. Secondly, the increase extents of the photocurrent amplitudes among the four kinds of WO_3 are different. Thirdly, the values of photogenerated current of the next cycle, in comparison with the former one, are lower. To illustrate these three points more clearly, the photocurrent values of each cycle in Fig.9 at the light turning off are extracted and depicted in Fig. 10(a). And the photogenerated current-time curves are shown in Fig. 10(b). Evidently, the current amplitudes of the four kinds of WO_3 films increase with the time increasing and the increasing ranges of the four kinds of WO_3 films are different. Meanwhile, the decreasing photogenerated current with time also can be found.

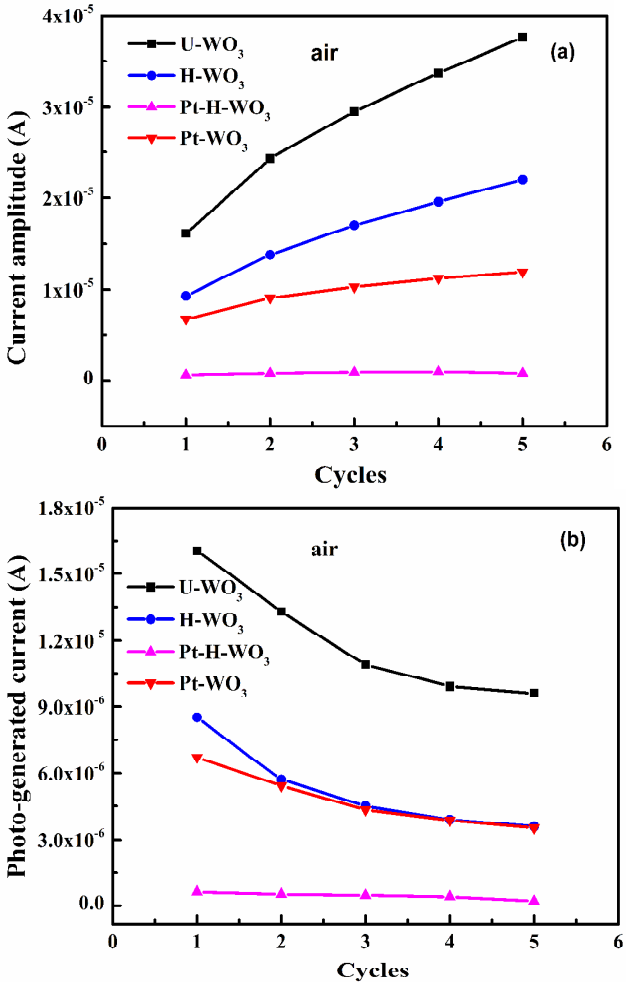

Fig. 10. The extracted photocurrent values of each cycle in Fig. 9 when turning the light off (a); the photo-generated current values of each cycle in Fig. 9 (b). U-WO_3 (untreated WO_3) films; H-WO_3 (hydrogen-treated WO_3) film; Pt-WO_3 (Pt-loaded WO_3) film and Pt-H-WO_3 (Pt-loaded hydrogenation WO_3) film.

For the first one, as all of the samples contain some oxygen vacancies which can trap electrons. The electrons trapped in the oxygen vacancies cannot contribute to the current, but the electrons photoexcited from the oxygen vacancies into the conduction band can raise the photocurrent [46]. During illumination, the electrons and holes are generated by absorbing the photon energy. Among them, some electrons are trapped by the oxygen vacancies. Removing the illumination, the trapped electrons cannot be completely released from the oxygen

vacancy. It means that some electrons are stored in the prior cycle. When the samples are exposed to the illumination again, electrons are excited from the valence band to the conduction band, meanwhile the electrons trapped in the oxygen vacancy levels can also be photoexcited into the conduction band contributing to the current. With the increase of test time, the number of electrons stored in the oxygen vacancies increases gradually until the oxygen vacancies existing in the WO_3 have been filled. Therefore, after being illuminated several times, the photocurrent curve of the samples presents the ladder-like increase.

For the second one, due to the different treatment processes, the four kinds of WO_3 films show different photocurrent response characteristics. In this section, we focus on the band bending effect between the WO_3 and its influence on the photoresponse processes. The characterization results verify that the four kinds of WO_3 surfaces are oxygen-deficient and, thus, n-type because of the excess electrons in the lattice-oxygen vacancies on the surface, which increase the electronic potential energy near the surface, causing the bands to bend upward. Meanwhile, when the metal and semiconductor are in contact, the band bending also happens. This is because that the free electrons will transfer between metal and semiconductor due to the work function difference [47]. Here, Pt with low lying Fermi level is a good acceptor of electrons from WO_3, which contributes to upward band bending [30]. In this way, a space charge region forms, resulting in the free charge carrier concentration near the semiconductor surface to be depleted compared with the bulk. It is widely accepted that the electron depletion region plays an important role in the producing of the photocurrent [13]. In the depletion region, the carrier mobility is suppressed due to the existence of the potential barrier. Only these electrons pass over the grain boundary, they can contribute to the current. The potential barrier dependence of the conductivity is given by

$$\sigma = ne\mu^* = ne\mu_0 \exp(\frac{-\phi_B}{k_B T}) = ne\mu_0 \exp(-\frac{qV}{k_B T}) \quad (1)$$

where n is the number of free carries, and μ^* and μ_0 are the effective mobility over the sample and the intrinsic mobility inside the grain, ϕ_B is the potential barrier, k_B is the Boltzmann constant, V is the energy band bending degree and T is the temperature. This equation means that the σ decreases with the V increasing. To understand the photoconductivity mechanism and explain the distinctive difference of the photocurrent responses among the four kinds of WO_3 films, the double Schottky barrier models of the two films are depicted in Fig. 11. As shown in the Fig. 11, upon blue irradiation, photogenerated holes and electrons are produced, and then they are separated under the effect of the built-in electric fields. In this process, some electrons are stored in the oxygen vacancies and transport from WO_3 to Pt that make the number of electrons in the conduction band lower than that of holes in the valence band. Combining the roles of the oxygen vacancies and Pt, the degrees of the band bending of the four samples are different. The order of the V is: Pt-H-WO_3 > Pt-WO_3 > H-WO_3 > U-WO_3. Therefore, the order of photocurrent amplitudes of the four kinds of WO_3 films is: U-WO_3 > H-WO_3 > Pt-WO_3 >Pt-H-WO_3.

For the third one, as the oxygen vacancy capturer is not occupied by photogenerated electrons before the reproducible photocurrent response tests, the number of the unoccupied oxygen vacancies is the largest, but as the testing proceeds, the oxygen vacancies are filled up by the electrons gradually. And the captured electrons cannot be completely released from the trap level during the period of turning the light off and before turning the light on. That is, some oxygen vacancies are still occupied by electrons. These electrons don't recombine with the holes in the valence band, therefore some holes still exist in the valence band. It means that in the next cycle when the light is on, the number of electrons excited from the valence band to the conduction band decreases. Therefore, the photo-generated current decreases with the time. Here, we use the first cycle and the second cycle as an example to illustrate these processes that are depicted in the Fig. 12. In these processes a range of reactions happen [5].

Under light irradiation, electron–hole pairs are generated [reaction (2)]. In this process, electrons are continually ejected into the conduction band (CB) and holes are generated in the valence band (VB). For these photogenerated electrons, some are captured by oxygen vacancies [reaction (3)]; some recombine with the holes; some contribute to the conductivity. When the light is off, the recombination of electrons and holes dominates, which makes the photocurrent decay. Considering some electrons are captured by the oxygen vacancies, they must first be excited into the conduction band and then recombine with holes. Therefore, the recombination process contains two processes, including reaction (4) and reaction (5).

$$WO_3 + h\nu \rightarrow WO_3^* + e^- + h^+ \quad (2)$$

$$e^- + trap \rightarrow e^-(Trap) \quad (3)$$

$$e^- + h^+ \rightarrow recombination(Heat) \quad (4)$$

$$e^-(Trap) + h^+ \rightarrow recombination(Heat) \quad (5)$$

In the first cycle, some electrons are stored in the oxygen vacancy and can't be totally released from the trap level. Thus some holes must exist in the valence band. When the second cycle starting, the number of electrons exciting from valence band to conduction band decreases under the same light illumination. Therefore, the photo-generated current decreases with the time.

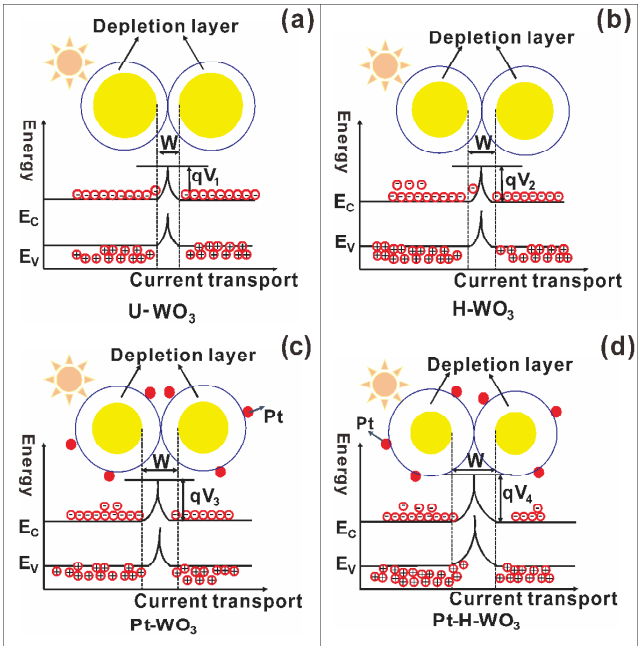

Fig. 11. The scheme of double Schottky barrier models of the four kinds of the films under blue light irradiation. E_c is the bottom of the conduction band, E_v is the top of the valence band, q is the electron charge, and V_i (i =1, 2, 3, 4) is the height of grain boundary barrier, W is the width of depletion layer. U-WO_3 (untreated WO_3) films (a); H-WO_3 (hydrogen-treated WO_3) film (b); Pt-WO_3 (Pt-loaded WO_3) film (c); and Pt-H-WO_3 (Pt-loaded hydrogenation WO_3) film (d).

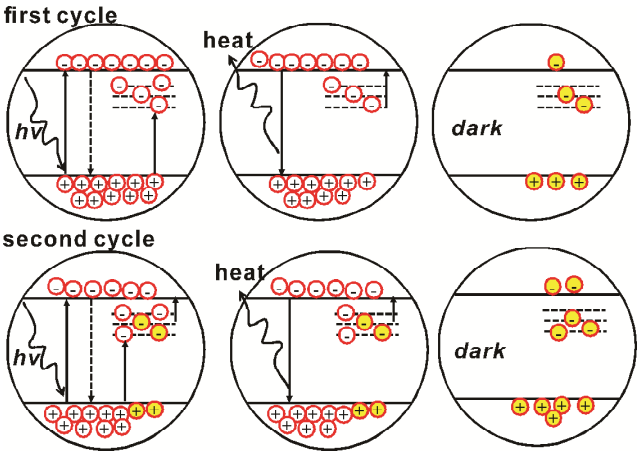

Fig. 12. Schematic illustrating the production process of the photo-generated electrons.

It is well known that photocurrent has been regarded as the most efficient method to evaluate the photocatalytic activity of composite photocatalyst [3,48]. But we should note that there is no direct relation between photocatalytic activity and photocurrent which is verified by Liu and his coworkers [15]. Inspired by the work of Liu et al., the formaldehyde is introduced into the test chamber to study the coupled effect of oxygen vacancy and Pt on the photoelectric responses of the four samples in formaldehyde. And the photocurrent- time curves are shown in the Fig. 13 (a). First, from an overall perspective, no matter in the air or in the formaldehyde, they have the same response shapes. Nevertheless the response amplitudes are different. Comparative analysis of the photocurrent responses in air and in formaldehyde, it is clearly found that the four samples all exhibits much higher photocurrent in formaldehyde than that in air. Zhang et al. reported that the adsorption of donor molecules on the semiconductor surface would bend the energy bands downward [46].When the four samples are tested in formaldehyde, the formaldehyde molecules donate electrons to the WO_3 causing downward band bending, which decreases the potential barrier. Meanwhile, we should also note that a series of reactions occur in formaldehyde. In addition to reactions (2) – (5), the reactions (6) – (9) also occur in formaldehyde as follows.

$$h^+ + H_2O(ads) \rightarrow H^+ + \bullet OH \quad (6)$$

$$O_2 + 2H^+ + 2e^- \xrightarrow{Pt} H_2O_2 \quad (7)$$

$$H_2O_2 + e^- \rightarrow OH^- + \bullet OH \quad (8)$$

$$HCHO + 2 \bullet OH \rightarrow CO_2 + H_2O + 2H^+ + 2e^- \quad (9)$$

As shown in the reaction (9), some electrons can be released. Therefore, the number of free carries of the four samples in formaldehyde is all more than that in air. According to the equation (1), the photocurrent increases with the decreasing of potential barrier and the increasing of electron. Therefore, the photocurrent in the formaldehyde is higher than that in the air.

Secondly, to illustrate the coupled effect of oxygen vacancy and Pt, the photocurrent amplitudes at each cycle in Fig. 9 and Fig. 13(a) are extracted, and their ratios defined as sensitivity are calculated. The ration is shown in the Fig. 13(b). From Fig. 13(b), it is obviously found that the sensitivity of Pt-H-WO_3 reached to 15.8 which is nearly 15 times higher than that of others at the first 300 s. We attribute it to the synthetic action of oxygen vacancies and Pt.

As we all know, the CB level of WO_3 (+0.5 V vs NHE) is more positive than the potentials for the single-electron reduction of oxygen ($O_2 + e^- = O_2^-(aq), -0.284 V vs NHE$; $O_2 + e^- + H^+ = HO_2(aq), -0.046 V vs NHE$) [35], the WO_3 films can't be allowed to efficiently consume photoexcited electrons. However, Pt can act as cocatalyst promoting the multielectron reduction of O_2. Therefore, reactions (2)-(9) all occur for Pt-WO_3 and Pt-H-WO_3. Although the electrons captured by Pt could recombine with the holes in air, the electrons can react with formaldehyde adsorbed on the surface of the Pt. This implies that Pt-loading can enhance the photocatalytic activity of WO_3 and H-WO_3 through facilitating both OH• and holes decomposition of organic compounds by promoting multielectron O_2 reduction. At the same time, we must pay attention to the fact that there are more oxygen vacancies in the Pt-H-WO_3.The presence of oxygen vacancies on the surface will facilitate formaldehyde adsorption [41]. This can not only reduce the energy barrier to increase the electron transport mobility, but also can promote the reaction (9) to increase the electron concentration. Meanwhile, as a result of the existence of Pt, the formaldehyde gases will spill over and replace the positions of •OH and react with the •OH in the same neighborhood. This is the same process of releasing electrons which can contribute to the photocurrent in the formaldehyde. And, From Fig. 13(a) and Fig. 9, the change rate of Pt-H-WO_3 is

obvious better than that of Pt-WO_3. This shows that the hydrogenation has an irreplaceable role on the gas sensing properties of the materials. Thus, we think it is the spill over model and oxygen vacancy theory that activate the sensitization in formaldehyde. The ratio of photocurrent in air to that in pollutant ambience can be used as an index to evaluate the photocatalytic activity [21]. Therefore, we can deduce that the photocatalytic activity of the Pt-H-WO_3 is the highest among the four kinds of WO_3 films. It also once again verifies that there is no direct relationship between photocurrent and photocatalytic activity.

At the same time, it's worth noting that the ration of $I_{formaldehyde}/I_{air}$ of the four samples increases with time increasing. We discuss this issue from the following two aspects. The first is the adsorption capacities of formaldehyde. With the time growing, the absorbed formaldehyde molecules increase gradually until the adsorption sites are filled up. The second is the electrons stored in the oxygen vacancies and Pt increase with the time growing and these electrons can be released to involve in reaction (9), which makes the ration of $I_{formaldehyde}/I_{air}$ increase with time. Among them, the Pt-H-WO_3 exhibits the most obvious increasing trend.

This is attributed to the synergistic effect of oxygen vacancy and Pt. For Pt-H-WO_3, the oxygen vacancies are abundant, therefore it can trap the most electrons and absorb the most formaldehyde molecules. Meanwhile Pt can promote the reaction (9) and facilitate the stored electrons to participate in the reaction (6)-(9). Therefore, the Pt-H-WO_3 exhibits the most obvious increasing trend.

Li et al. have reported that Pt-H-WO_3 still has some catalytic properties to formaldehyde under dark condition [9]. Inspired from this, we want to know whether there is a current response existing in the four kinds of WO_3 films under dark condition in air and in formaldehyde, respectively. Therefore, the dark responses of the four kinds of WO_3 films were investigated. For the four samples, no response was found in air, which was not shown in the paper, while the obvious response in the formaldehyde was found, which is shown in Fig. 14. From Fig. 14, it can be seen that the U-WO_3 and H-WO_3 exhibit the same response models. Meanwhile, the Pt-WO_3 and Pt-H-WO_3 show the same response models.

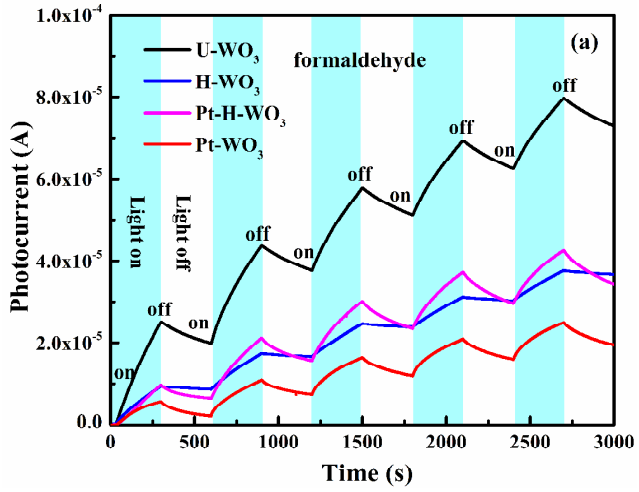

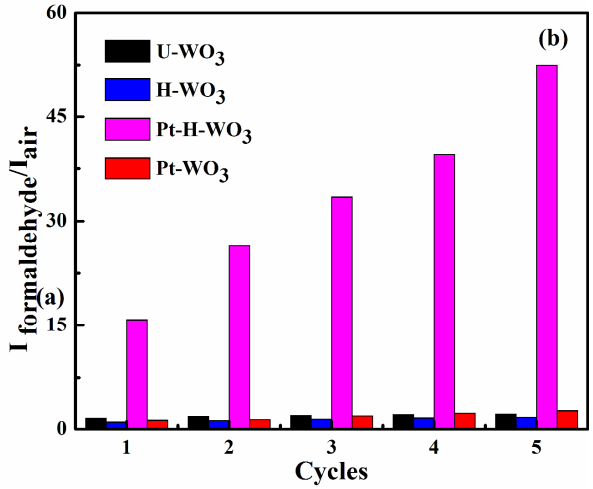

Fig. 13. Photocurrent-time curves of the four samples in formaldehyde under blue light illumination (a); the Sensitivity ($I_{formaldehyde}/I_{air}$) versus time (b). U-WO_3 (untreated WO_3) films; H-WO_3 (hydrogen-treated WO_3) film; Pt-WO_3 (Pt-loaded WO_3) film and Pt-H-WO_3 (Pt-loaded hydrogenation WO_3) film.

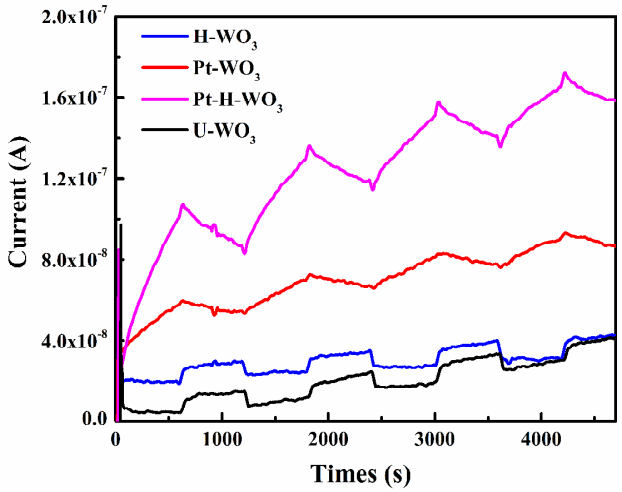

Fig. 14. Current-time curves of the four of WO_3 films to formaldehyde in the darkness. U-WO_3 (untreated WO_3) films; H-WO_3 (hydrogen-treated WO_3) film; Pt-WO_3 (Pt-loaded WO_3) film and Pt-H-WO_3 (Pt-loaded hydrogenation WO_3) film.

For U-WO_3 and H-WO_3 films, the current decreases once the formaldehyde is in and the current increases once the formaldehyde is out. However, the contrary is the case for Pt-WO_3 and Pt-H-WO_3 films. The current comes from the transportation of electrons stored in the WO_3. Because the formaldehyde molecules are polar molecules and WO_3 is the polar semiconductor, a dipole-dipole interaction will form in the interface when the formaldehyde molecules are absorbed on the surface of WO_3 films. When the electrons transfer between the WO_3 nanoparticles to form current, they must overcome the dipole-dipole interaction [49]. Therefore, the current values of U-WO_3 and H-WO_3 shown in Fig. 14 decrease immediately once the formaldehyde gas is bubbled into the test chamber. While when the formaldehyde gas is out, the dipole-dipole interaction is weakened, thus the current of U-WO_3 and H-WO_3 increases. For

Pt-WO_3 and Pt-H-WO_3, the situations are different. Although the dipole-dipole interactions still exist between WO_3 and formaldehyde molecules, chemical reactions with the help of Pt play major roles. It means that the effect of the dipole-dipole interactions can be ignored in the Pt-WO_3 and the Pt-H-WO_3. Recently, it has been reported that the presence of Pt on WO_3 is known to facilitate the multielectron reduction of O_2 resulting in producing OH radicals [40]. In our work, although no photogenerated electrons and holes are generated under dark condition, the energy stored in the WO_3 with the help of Pt can be released, which provide a support for the reaction (7)-(9). Therefore, we can see the current responses of the Pt-WO_3 and the Pt-H-WO_3 in dark. As more energy stored and more active sites existing in the Pt-H-WO_3 compared with Pt-WO_3, thus the response of Pt-H-WO_3 is higher than that of Pt-WO_3.

4 Conclusions

In this work, the microstructures of the four WO_3 films were characterized systematically and the photoelectric response characteristics of the four WO_3 films were tested centrally. We focus on the influences of Pt and oxygen vacancies on the photoelectric responses of WO_3 films in dark and light conditions at room temperature. The Pt-loaded hydrogenation WO_3 shows the highest sensitivity to the formaldehyde under radiation and the most obvious response in dark. The results demonstrated that coupling of oxygen vacancy and Pt has a certain research value. In this work, the oxygen vacancies can provide trapping sites to trap electrons to be stored, prolonging the life of the carriers, which can suppress recombination of electrons with holes and provide active sites to absorb formaldehyde enhancing the gas sensitive values. Meanwhile, Pt can act as an electron sink to capture, store electrons transferring from excited semiconductors and act as a recombination center to facilitate the recombination of the electrons and holes. The coupled effect of oxygen vacancy and Pt cannot change the photoelectric response shapes, but can change the response amplitude and sensitivity through modulating the band bending and chemical reactions. This work may be of great value in developing new sensitive material for detection of pollution gases without energy consumption and new method for modulation of the material properties.

Acknowledgements

This work was supported by Nature Science Foundation of China (No. 50927201) and the National Basic Research Program of China (Grant Nos. 2009CB939705 and 2009CB939702). The authors are also grateful to Analytical and Testing Center of Huazhong University of Science and Technology.

Notes and references

State Key Laboratory of Material Processing and Die & Mould Technology, Nanomaterials and Smart Sensors Research Laboratory, Department of Materials Science and Engineering, Huazhong University of Science and Technology, Wuhan 430074, PR China. Fax: +86-27-8754-3778; Tel: +86-27-8755-6544; E-mail: csxie@mail.hust.edu.cn (Changsheng Xie).

1 J. P. Zou, Q. Zhang, K. Huang and N. Marzari, J. Phys. Chem. C, 2010, 114, 10725–10729.
2 R. X. Li, Q. Yue and Z. M. Wei, J. Mater. Chem. C, 2013, 1, 5866-5877.
3 H.-i. Kim, J. Kim, W. Kim and W. Choi, J. Phys. Chem. C, 2011, 115, 9797-9805.
4 J. Nelson, A. M. Eppler and I. M. Ballard, J. Photochem. Photobiol. A: chem., 2002, 148, 25-31.
5 C. Q. Yang, Q. Zhu, S. P. Zhang, Z. J. Zou, K. Tian, C. S. Xie, Appl. Surf. Sci., 2014, 297, 116-124.
6 N. J. Huo, S. X. Yang, Z. M. Wei and J. B. Li, J. Mater. Chem. C, 2013, 1, 3999-4007.
7 L. L. Shi, F. Wang, B. H. Li, X. Chen, B. Yao, D. X. Zhao and D. Z. Shen, J. Mater. Chem. C, 2014, 2, 5005–5010.
8 X. B. Chen, L. Liu, P. Y. Yu and S. S. Mao, Sci., 2011, 331, 746-750.
9 J. Li, Y. Liu, Z. J. Zhu, G. Z. Zhang, T. Zou, Z. J. Zou, S. S. Zhang and D. W. Zeng, C. S. Xie, Sci. Rep., 2013, 3, 02409.
10 Q. Zhu, C. S. Xie, H. Y. Li, C. Q. Yang, S. S. Zhang and D. W. Zeng, J. Mater. Chem. C, 2014, 23, 4566 - 4580.
11 R. Solarska, A. Królikowska and J. Augustyński, Angew. Chem. Int. Ed., 2010, 49, 7980-7983.
12 W. J. Lee, P. S. Shinde, G. H. Go and E. Ramasamy, Int. J. Hydrogen. Energy, 2011, 36, 5262-5270.
13 Y. Muraoka, N. Takubo and Z. Hiroi, J. Appl. Phys., 2009, 105, 103702.
14 T. Tsurumi, S. Nishizawa, N. Ohashi and T. Ohgaki, Jpn. J. Appl. Phys., 1999, 38, 3682.
15 Z. J. Zou, C. S. Xie, S. S. Zhang, C. Q. Yang, G. Z. Zhang, L. Yang , Sens. Actuators B: Chem., 2013, 188, 1158-1166.
16 A. Stevanovic, M. Buttner, Z. Zhang and J. T. Yates, Jr., J. Am. Chem. Soc., 2012, 134, 324-332.
17 A. Zangwill, Physics at surfaces, Cambridge University Press, 1988.
18 N. A. Galiote, R. L. T. Parreira, J. M. Rosolen and F. Huguenin, Electrochem. Commun., 2010, 12, 733-736.
19 D. S. Dalavi, R. S. Devan, R. A. Patil, R. S. Patil, Y.-R. Ma, S. B. Sadale, I. Kim, J.-H. Kim and P. S. Patil, J. Mater. Chem. C, 2013, 1, 3722.
20 Y.-G. Choi, G. Sakai, K. Shimanoe, N. Miura and N. Yamazoe, Sens. Actuators B: Chem., 2003, 95, 258-265.
21 X. Q. An, J. C. Yu, Y. Wang, Y. M. Hu, X. L. Yu and G. J. Zhang, J. Mater. Chem., 2012, 22, 8525.
22 J. J. Guo, Y. Li, S. M. Zhu, Z. X. Chen, Q. L. Liu, D. Zhang, W.-J. Moon and D.-M. Song, RSC Adv., 2012, 2, 1356-1363.
22 Y. Liu, C. S. Xie, J. Li, T. Zou and D. W. Zeng, Appl. Catal. A: gen., 2012, 433-434, 81-87.
23 Z. L. Xu, I. Tabata, K. Hirogaki, K. Hisada, T. Wang, S. Wang and T. Hori, Mater. Lett., 2011, 65, 1252-1256.
24 G. M. Wang, Y.C. Ling, H.Y. Wang, X.Y. Yang, C.C. Wang, J.Z. Zhang and Y. Li, Energy Environ. Sci., 2012, 5, 6180-6187.
25 A. Memar, W.R.W. Daud, S. Hosseini, E. Eftekhari and L.J. Minggu, Sol. Energy, 2010, 84, 1538-1544.
26 K.H. Yoon, D.K. Seo, Y.S. Cho and D.H. Kang, J. Appl. Phys. 1998. 84,f 3954.
27 Q. Zhu, C. S. Xie, H. Y. Li and C. Q. Yang, J. Alloy. Compd., 2014, 585, 267-276.
28 J. Yang, W. Li, J. Li, D. Sun and Q. Chen, J. Mater. Chem., 2012, 22, 17744-17752.
29 H.Y. Li, C.S. Xie, Y. C. Liao, Y. Liu, Z.J. Zou and J. Wu, J. Alloy. Compd., 2013, 569, 88-94.
30 L. Cheng, Y. Hou, B. Zhang, S. Yang, J. W. Guo, L. Wu and H. G. Yang, Chem. Commun., 2013, 49, 5945-5947.
31 S.S. Kalanur, Y.J. Hwang, S.Y. Chae and O.S. Joo, J. Mater. Chem. A, 2013, 1, 3479-3488.
32 J. P. Wang, Z. Y. Wang, B. B. Huang, Y. D. Ma, Y. Y. Liu, X. Y. Qin, X. Y. Zhang and Y. Dai, ACS Appl. Mater. Interfaces, 2012, 4, 4024-4030.
33 J.Y. Luo, S.Z. Deng, Y.T. Tao, F.L. Zhao, L.F. Zhu, L. Gong, J. Chen and N.S. Xu, J. Phys. Chem. C, 2009, 113, 15877-15881.

34 J.Y. Luo, N.S. Xu, F.L. Zhao, S.Z. Deng and Y.T. Tao, J. Appl. Phys., 2011, 109, 024312.
35 A. Sonia, Y. Djaoued, B. Subramanian, R. Jacques, M. Eric, B. Ralf and B. Achour, Mater. Chem. Phys., 2012, 136, 80-89.
36 Y.S. Zou, Y.C. Zhang, D. Lou, H.P. Wang, L. Gu, Y.H. Dong, K. Dou, X.F. Song and H.B. Zeng, J. Alloy. Compd., 2014, 583, 465-470.
37 A. Shpak, A. Korduban, M. Medvedskij and V. Kandyba, J. Electron Spectrosc. 2007, 156, 172-175.
38 C. Navío, S. Vallejos, T. Stoycheva, E. Llobet, X. Correig, R. Snyders, C. Blackman, P. Umek, X. Ke and G. Van Tendeloo, Mater. Chem. Phys., 2012, 134, 809-813.
39 K. Patel, C. Panchal, M. Desai and P. Mehta, Mater. Chem. Phys., 2010, 124, 884-890.
40 H. W. Park, K. B. Chung and J. S. Park, Curr. Appl. Phys., 2012, 122, S164-S167.
41 X. Pan, M.-Q. Yang, X. Fu, N. Zhang and Y.-J. Xu, Nanoscale, 2013, 5, 3601-3614.
42 M. W. Ahn, K. S. Park, J. H. Heo, J. G. Park, D. W. Kim, K. J. Choi, J. H. Lee and S. H. Hong, Appl. Phys. Lett., 2008, 93, 263103.
43 Y. Liu, C. S. Xie, H. Y. Li, H. Chen, T. Zou and D. W. Zeng, J. Hazard. Mater. 2011, 196, 52-58.
44 A. Takai and P.V. Kamat, Acs Nano, 2011, 5, 7369-7376.
45 A. Bera and D. Basak, Appl. Phys. Lett. 2009, 94, 163119-163113.
46 J. Y. Gan, X. H. Lu, J. H. Wu, S. L. Xie, T. Zhai, M. H. Yu, Z. S. Zhang, Y. C. Mao, S.C.I. Wang, Y. Shen and Y. X. Tong, Sci. Rep., 2013, 3.
47 Z. Zhang and J.T. Yates Jr, Chem. Rev., 2012, 112, 5520−5551.
48 B. Yang, P. R. F. Barnes, W. Bertram and V. Luca, J. Mater. Chem., 2007, 17, 2722-2729.
49 A. Oprea, N. Bârsan and U. Weimar, Sens. Actuators B: Chem., 2009, 142(2), 470-493.

The coupled effect of oxygen vacancy and Pt on the photoelectric response of tungsten trioxide films

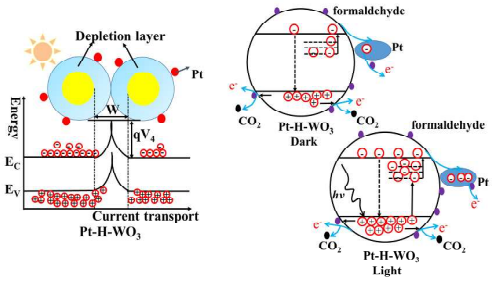

The coupled of Pt and oxygen vacancy make the Pt-H-WO_3 show excellent sensitivity to formaldehyde in light or in dark.